Circuit approach to the minimal configuration of terahertz anomalous extraordinary transmission

M. Beruete' , M. Navarro-Cía' , S. A. Kuznetsov' , and M. Sorolla'

Citation: Appl. Phys. Lett. **98**, 014106 (2011); doi: 10.1063/1.3533815
View online: http://dx.doi.org/10.1063/1.3533815
View Table of Contents: http://aip.scitation.org/toc/apl/98/1
Published by the American Institute of Physics

Circuit approach to the minimal configuration of terahertz anomalous extraordinary transmission

M. Beruete,[1,a)] M. Navarro-Cía,[1,b)] S. A. Kuznetsov,[2,c)] and M. Sorolla[1,d)]
[1]*Millimeter and Terahertz Waves Laboratory, Universidad Pública de Navarra, E-31006 Pamplona, Spain*
[2]*Research-and-Education Centre "Nanosystems and Modern Materials," Novosibirsk State University, Pirogova Str. 2, 630090 Novosibirsk, Russia and Budker Institute of Nuclear Physics SB RAS, Lavrentiev Ave. 11, 630090 Novosibirsk, Russia*

(Received 14 October 2010; accepted 11 December 2010; published online 7 January 2011)

In this letter we present an in-depth circuit analysis of anomalous extraordinary transmission (ET) through subwavelength slit and hole arrrays loaded by a dielectric slab. We show the key role played by the thickness of the dielectric slab in order to enhance the transmission for TE-polarized waves (incident electric field parallel to the slits or to the short in-plane period in hole arrays arranged in rectangular lattice) within the cut-off regime of the apertures and to suppress Wood's anomaly. Analytical and numerical results together with experimental data are presented, showing good agreement among them. This work provides physical insight of the underlying mechanism governing anomalous ET and offers further independent control over orthogonal polarized waves impinging into subwavelength aperture arrays. © *2011 American Institute of Physics*.
[doi:10.1063/1.3533815]

Transmission through subwavelength apertures[1] has attracted a great deal of interest since the first report of extraordinary transmission (ET).[2] Although initially found in the near infrared, it was then measured in other frequency ranges, even when metals are nearly perfect conductors,[3] so the general underlying mechanism is related to the diffraction modes of the periodic structure.[4,5] Nowadays, ET has evolved extensively giving birth to interesting applications such as molecular sensing, near-field scanning optical microscopy, nonlinear optics, etc.[6] Furthermore, the terahertz gap is experiencing a spectacular increment of sensing and imaging applications due to the nonionizing character of radiation at these frequencies that make them of great interest for biological as well as security issues.[7]

In the past, we reported terahertz-ET employing hole arrays in a rectangular lattice on a polypropylene film.[8] We also detected a high transmission peak below cut-off when the electric field was parallel to the short hole array periodicity, although, in principle, the shorter periodicity should forbid ET. Consequently, it was termed anomalous ET. The physical explanation is closely related to the excitation of a dielectric slab mode.[4,8] Similar results were theoretically discussed for slit arrays.[9]

Here we present a circuit analysis of anomalous ET through hole arrays and inductive slit arrays similar to the one presented in Ref. 10 to analyze capacitive slit arrays. Equivalent circuits for regular ET were presented in Refs. 11 and 12.

For the analysis, the problem is reduced to a single unit cell with orthogonal electric and magnetic walls,[11] see Fig. 1(a). An inductive aperture (circular in the plot) backed by a dielectric slab is inserted in the middle section of the waveguide. In the subsequent analysis the normalized hole diameter (slit width) is $a/d_x=0.35$ and the ratio between lattice dimensions is $d_y/d_x=0.4$.

From the artificial waveguide, the equivalent circuit of Fig. 1(b) is deduced (see caption for notation). There are fundamental differences with respect to Ref. 10. A small hole or a vertical slit on a metallic plate has an inductive nature[13] and the first higher order mode of the artificial waveguide is the TE_{20} mode, rather than TM_{02}, whose admittance is

$$Y_{TE_{20}}=\sqrt{\varepsilon}\sqrt{1-\left(\frac{f_c}{f}\right)^2}=\begin{cases}-j\sqrt{\varepsilon}\sqrt{\left(\frac{f_c}{f}\right)^2-1} & f<f_c\\ \sqrt{\varepsilon}\sqrt{1-\left(\frac{f_c}{f}\right)^2} & f\geq f_c,\end{cases} \quad (1)$$

where $f_c=c/(d_x\sqrt{\varepsilon})$ is the cut-off frequency in a medium with permittivity ε, c the speed of light in vacuum, and d_x the horizontal waveguide dimension. Below cut-off, the inductive character of the admittance is explicitly shown. In the unloaded case, the equivalent circuit reduces to a transversal electromagnetic (TEM) transmission line loaded with three shunt inductive admittances $[Y_{ap}+2C^{air}Y^{air}_{TE_{20}}$, where C^{air} is the coupling coefficient between the fundamental TEM and the TE_{20} mode] and no resonant peak of transmission can be expected. This is even more obvious when the aperture is a vertical slit since in that case the invariance along y prevents the excitation of TM modes and then all the parallel elements are inductive. These features are shown in the curves of Fig. 2 labeled as $F=0$ where the simulated (dashed) as well as analytical (solid) transmission coefficients of freestanding slit [panel (a)] and hole [panel (b)] arrays are compared. Numerical results were obtained with CST MICROWAVE STUDIO™, and the agreement with the equivalent circuit results is outstanding.

When a dielectric slab is added, the parallel admittances due to the TE_{20} mode modify accordingly. With a single dielectric slab backing the perforated plate, with the rest of the waveguide filled with air, the admittance due to TE_{20} mode is

a)FAX: +34948169720. Electronic mail: miguel.beruete@unavarra.es.
b)Electronic mail: miguel.navarro@unavarra.es.
c)Electronic mail: s.a.kuznetsov@inp.nsk.su.
d)Electronic mail: mario@unavarra.es.

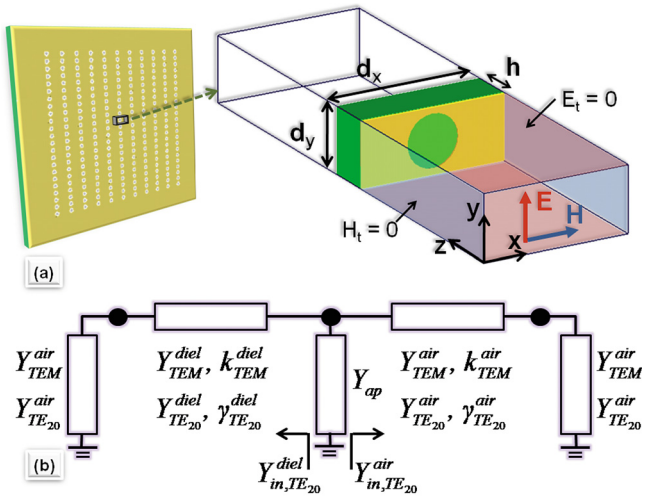

FIG. 1. (Color online) (a) Schematic representation of the equivalent waveguide employed to analyze anomalous ET. The location of electric and magnetic planes is consistent with the wave polarization. Parameters: d_x, d_y in-plane periodicities; h dielectric slab thickness of permittivity ε. (b) Equivalent circuit where the previous waveguide is reduced to two dominant modes: TEM and TE_{20}. Notation: subscripts denote the specific mode (TEM or TE_{20}) and superscripts the medium (air or dielectric); γ_i^j (i: TEM/TE_{20}; j: air/diel) is the complex propagation constant, which in the case of TEM mode reduces to $k_{\mathrm{TEM}}^{\mathrm{air}}=k_0$ and $k_{\mathrm{TEM}}^{\mathrm{diel}}=\varepsilon k_0$; Y_i^j and $Y_{\mathrm{in},i}^j$ are the characteristic and input admittances in each case.

$$Y_{\mathrm{in,TE_{20}}} = C^{\mathrm{diel}} Y_{\mathrm{TE_{20}}}^{\mathrm{diel}} \frac{Y_{\mathrm{TE_{20}}}^{\mathrm{air}} + Y_{\mathrm{TE_{20}}}^{\mathrm{diel}} \tanh\left[\sqrt{\left(\frac{2\pi}{d_x}\right)^2 - \varepsilon k_0^2}\, h\right]}{Y_{\mathrm{TE_{20}}}^{\mathrm{diel}} + Y_{\mathrm{TE_{20}}}^{\mathrm{air}} \tanh\left[\sqrt{\left(\frac{2\pi}{d_x}\right)^2 - \varepsilon k_0^2}\, h\right]} + C^{\mathrm{air}} Y_{\mathrm{TE_{20}}}^{\mathrm{air}}, \tag{2}$$

where the first and second terms on the right-hand side correspond to the input admittance seen toward the source and load, respectively, and C^{diel} and C^{air} stand for the coupling coefficients between the fundamental TEM mode and the TE_{20} mode in the dielectric loaded and air faces, respectively. It is assumed that the only relevant higher order mode is the TE_{20} and we assume that the rest of higher order TE modes simply add an inductance that we insert in the term Y_{ap} of Fig. 1(b). The effect of TM modes is neglected, which is a reasonable approximation in rectangular structures where $d_x > 2d_y$. Inevitably, this leads to inaccuracies above f_c^{air} ($=c/d_x$), which will be more evident in hole arrays than in slit arrays where TM modes play no role at all. According to Eq. (2) three different spectral regions can be identified. When $f < f_c^{\mathrm{diel}}[=c/(d_x\sqrt{\varepsilon})]$ the input admittance is purely inductive and when $f > f_c^{\mathrm{air}}$ the admittance is in general complex and the first term of the right-hand side does not show any pole, so no resonant features are foreseen in either case.

Interestingly, when $f_c^{\mathrm{diel}} < f < f_c^{\mathrm{air}}$ the input admittance $Y_{\mathrm{in,TE_{20}}}$ is purely imaginary and the term due to the dielectric slab $Y_{\mathrm{in,TE_{20}}}^{\mathrm{diel}}$ can have poles and zeros. In the most general scenario, a zero takes place first, and then a pole emerges. Nevertheless, depending on the dielectric slab parameters, the latter would effectively occur above f_c^{air}. Defining an auxiliary factor $F=h\sqrt{\varepsilon-1}/d_x$, if $F \geq 0.25$ (curve labeled as $F=0.34$ in Fig. 2) then $f_c^{\mathrm{diel}} < f_{\mathrm{pole}} < f_c^{\mathrm{air}}$ and there is a frequency where the admittance diverges to infinity originating a null in transmission (known as Wood's anomaly in grating theory). The pole is preceded by a zero that changes the sign

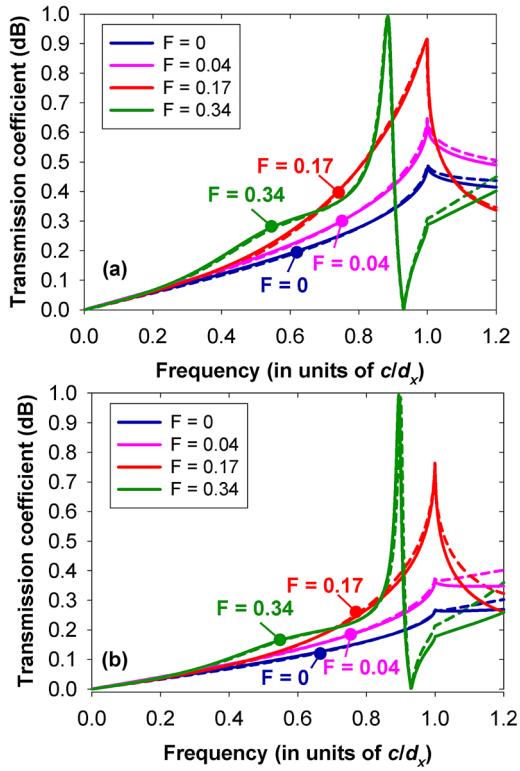

FIG. 2. (Color online) Anomalous ET for subwavelength slit (a) and hole (b) arrays. Numerical simulation (dashed) and equivalent circuit (solid) results for $F=0$ (unloaded structure), $F=0.04$, $F=0.17$, and $F=0.34$.

of the admittance that becomes capacitive. The pole makes the capacitance tend to infinity so there is a frequency where it completely cancels the total inductance due to the aperture and $Y_{\mathrm{in,TE_{20}}}^{\mathrm{air}}$. Thus, the null in transmission is related to a resonance of the TE_{20} mode in the dielectric slab and the peak is a consequence of the strong admittance divergence associated with the resonance that eventually matches the aperture inductance. Other features observed in the figure are the slight crest before the anomalous ET peak, caused by the constructive interference due to the Fabry–Pérot resonance of the fundamental TEM wave inside the dielectric slab, and a kink at c/d_x related to the change from cut-off to propagation of the TE_{20} mode in air. Again a very good agreement is observed between the simulation (dashed) and equivalent circuit (solid) results and, as expected, the concordance is better for slit than for hole arrays.

Conversely, if $F<0.25$ no pole appears in the spectrum since this condition would be above f_c^{air}. However, this frequency is a branch point beyond which the admittance is no longer purely imaginary but complex. Nevertheless, a maximum is still possible, as $Y_{\mathrm{in,TE_{20}}}^{\mathrm{diel}}$ always has a zero (in the limit $F=0$ it appears exactly at f_c^{air}) so that $Y_{\mathrm{in,TE_{20}}}^{\mathrm{diel}}$ has capacitive character with a capacitance that increases monotonously (although not necessarily diverging to infinity due to the absence of a pole) and a point can exist where it still cancels the inductance. However, a closed analytical expression cannot be given since it depends on the exact geometry. At most, what can be expected is a relative maximum (a kink) at c/d_x, without the presence of a marked minimum (at difference of what happened with $F=0.34$) due to lack of any pole.

This case has been plotted in the curves of Fig. 2 labeled as $F=0.04$ and 0.17. Clearly, a local maximum appears in

TABLE I. Unit cell parameters of the three subwavelength hole arrays fabricated and measured in this work.

F	h (μm)	ε	d_x (μm)	d_y (d_y/d_x) (μm)	a (a/d_x) (μm)
0.04	40	2.25	1200	500 (0.42)	420 (0.35)
0.20	20	2.25	113	47.5 (0.42)	43.1 (0.38)
0.34	980	2.43	3400	1500 (0.44)	1200 (0.35)

both cases, and its magnitude approaches unity for the latter case. Also, the level is different in hole or slit arrays since both inductance and coupling factors are different in each situation. A good agreement is again noticed between simulation and equivalent circuit results.

In order to validate analytical and numerical results, subwavelength hole arrays with F factors covering the three cases studied were characterized. Table I summarizes unit cell parameters. Cases $F=0.04$ and 0.20 were manufactured by a conventional photolithography technique and measured with a backward-wave oscillator spectrometer and a vacuum Fourier transform-spectrometer "Bruker IFS 66v/s," respectively. The other case, $F=0.34$ was manufactured by a numerical milling machine and tested with an ABmm™ vector network analyzer.

Clearly, $F=0.04$ (Fig. 3) does not display any resonant feature, whereas the other cases do. Notice also that Wood's anomaly is slightly manifested for $F=0.34$ and suppressed for the other two cases in agreement with the previous analysis. Also, in the case of $F=0.34$, one can perceive the slight crest and the kink before and after the anomalous ET in that order. Moreover, the narrower behavior of the anomalous ET peak for $F=0.34$ with respect to $F=0.20$ is evident.

Total transmission is expected for $F=0.34$, but the transmission coefficient reaches a moderate value of 0.35, even lower than for $F=0.20$. This disagreement can be explained by the number of illuminated holes:[14] when $F=0.34$, the incident Gaussian beam impinges on the sample with a diameter of 18.4 mm illuminating effectively 72 holes (6×12), whereas when $F=0.20$, the Gaussian beam diameter is 10 mm and illuminates up to 18 480 holes (210×88). Also, the measured structure is obviously lossy, and due to the strongly resonant nature of the peak, intense electric currents are excited at resonance leading to Ohmic dissipation. In addition, manufacture tolerances cannot be discarded.

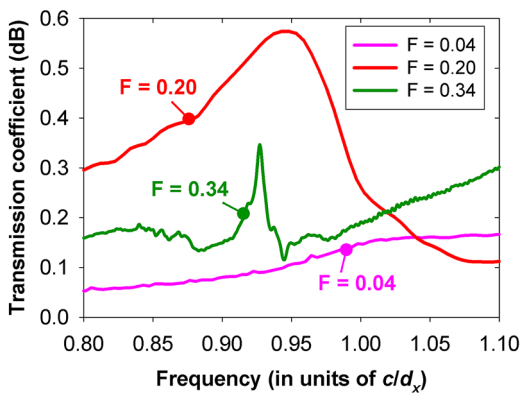

FIG. 3. (Color online) Experimental anomalous ET through three different subwavelength hole arrays: $F=0.04$, $F=0.20$, and $F=0.34$.

Ohmic losses can be easily included in the equivalent circuit by simply connecting a resistor in series with the aperture inductor. Nevertheless, it is not straightforward to incorporate the effect of the number of holes. This puts in evidence the main drawback of the circuit approach to characterize regular and anomalous ET: it does not account for effects caused by finite structure; thus, it may disagree with experimental results in terms of magnitude. Anyway, it is a useful tool to find the location of resonances and to predict rapidly anomalous ET and suppression of Wood's anomaly.

In summary, circuital analysis founded on transmission line concepts has been applied to model the anomalous ET through subwavelength apertures. Those regimes where anomalous ET happens have been identified with the excitation of the TE_{20} mode of the artificial waveguide. The zero and pole introduced by this mode when it is in propagation inside the slab are sufficient to explain the presence of peaks and nulls of transmission. A deep analysis of the different operation regimes as a function of the dielectric slab parameters has been presented: for thick enough substrates a peak followed by a null appears, whereas for thin substrates only the peak survives, being equivalent to an effective suppression of Wood's anomaly. The closed-form analytical formulas derived agree remarkably with full-wave numerical calculations and are also well-supported by experimental data at millimeter and terahertz waves. These closed-form analytical equations are useful as a fast design tool for applications such as dark field and near-field scanning optical microscopy[15] and filters sensitive to polarization.

The authors are grateful to Professor V. Lomakin from UCSD and Professor F. Medina from Universidad de Sevilla for the fruitful discussion. This work has been supported by the Spanish Government under contracts Consolider "Engineering Metamaterials" Grant Nos. CSD2008-00066 and TEC2008-06871-C02-01.

[1] A. Lewis, M. Isaacson, A. Harrontunian, and A. Muray, Ultramicroscopy **13**, 227 (1984).
[2] T. W. Ebbesen, H. J. Lezec, H. Ghaemi, T. Thio, and P. A. Wolf, Nature (London) **391**, 667 (1998).
[3] M. Beruete, M. Sorolla, I. Campillo, J. S. Dolado, L. Martín-Moreno, J. Bravo-Abad, and F. J. García-Vidal, Opt. Lett. **29**, 2500 (2004).
[4] V. Lomakin and E. Michielssen, Phys. Rev. B **71**, 235117 (2005).
[5] F. J. García-Vidal, L. Martín-Moreno, T. W. Ebbesen, and L. Kuipers, Rev. Mod. Phys. **82**, 729 (2010).
[6] R. Gordon, A. G. Brolo, D. Sinton, and K. L. Kavanagh, Laser Photonics Rev. **4**, 311 (2010).
[7] P. H. Siegel, IEEE Trans. Microwave Theory Tech. **52**, 2438 (2004).
[8] S. A. Kuznetsov, M. Navarro-Cía, V. V. Kubarev, A. V. Gelfand, M. Beruete, I. Campillo, and M. Sorolla, Opt. Express **17**, 11730 (2009).
[9] E. Moreno, L. Martín-Moreno, and F. J. García-Vidal, J. Opt. A, Pure Appl. Opt. **8**, S94 (2006).
[10] R. Rodríguez-Berral, F. Mesa, and F. Medina, Appl. Phys. Lett. **96**, 161104 (2010).
[11] M. Beruete, I. Campillo, M. Navarro-Cía, F. Falcone, and M. Sorolla, IEEE Trans. Antennas Propag. **55**, 1514 (2007).
[12] F. Medina, F. Mesa, and R. Marqués, IEEE Trans. Microwave Theory Tech. **56**, 3108 (2008).
[13] N. Marcuvitz, *Waveguide Handbook*, Electromagnetic Waves Series (P. Peregrinus on behalf of IEE, London, 1986).
[14] M. Beruete, M. Sorolla, I. Campillo, and J. S. Dolado, IEEE Microw. Wirel. Compon. Lett. **15**, 116 (2005).
[15] G. Zheng, X. Cui, and Ch. Yang, Proc. Natl. Acad. Sci. U.S.A. **107**, 9043 (2010).